MedChemComm

RSC Publishing

CONCISE ARTICLE

View Article Online
View Journal | View Issue

Cite this: *Med. Chem. Commun.*, 2013, **4**, 520

Synthesis and *in vitro*/*in vivo* pharmacological evaluation of [^{11}C]-ThioABP, a novel radiotracer for imaging mGluR5 with PET†

Selena Milicevic Sephton,[a] Linjing Mu,*[b] Adrienne Müller,[a] Cindy A. Wanger-Baumann,[a] Roger Schibli,[ab] Stefanie D. Krämer[a] and Simon M. Ametamey*[a]

Received 5th November 2012
Accepted 19th December 2012

DOI: 10.1039/c2md20332d

www.rsc.org/medchemcomm

We have designed a novel positron emission tomography (PET) radiotracer, [^{11}C]-ThioABP, a thiazole based derivative for imaging the metabotropic glutamate receptor subtype 5 (mGluR5), and prepared the hydroxy oxime precursor **4** in a 15% overall yield. [^{11}C]-ThioABP was radiosynthesized in the Veenstra module and obtained in a decay corrected radiochemical yield of 40% and specific activity of 80–250 GBq μmol^{-1} at the end of synthesis. ThioABP exhibited excellent binding affinity (K_i) *in vitro* of 1.9 ± 0.9 nM and [^{11}C]-ThioABP showed an optimal log $D_{7.4}$ of 2.4. The autoradiographic studies on rat brain slices revealed specific binding to mGluR5. *In vivo* evaluation of [^{11}C]-ThioABP including a displacement study with MMPEP in a dynamic PET scan showed a specificity of [^{11}C]-ThioABP for mGluR5. Radio-TLC metabolite studies showed a good metabolic stability of [^{11}C]-ThioABP *in vivo*. The comparison of biological properties of [^{11}C]-ThioABP and [^{11}C]-ABP688 revealed similarity between these two compounds.

Introduction

In recent years, positron emission tomography (PET) has emerged as a non-invasive molecular imaging technique capable of facilitating drug development through quantification of biochemical and pharmacological parameters. The further advancement of the PET imaging modality is among other factors dependent on the development of new PET radiotracers which specifically and selectively bind to their biological targets of interest. PET radiotracers can be any bioactive or synthetic molecules labelled with positron emitting nuclide (*e.g.*, fluorine-18 or carbon-11).[1] Most commonly, extensive structure–activity relationship (SAR) studies are required for identification of new PET radiotracers and one such successful example is an SAR study for the establishment of [^{11}C]-ABP688 (Fig. 1).[2–4] To date, [^{11}C]-ABP688 is the most successful clinically applied PET radiotracer for imaging metabotropic glutamate receptor subtype 5 (mGluR5) in human subjects.[5–12] Our particular interest in mGluR5 arose from its involvement in several central nervous system (CNS) diseases (*e.g.*, Parkinson's and Alzheimer's diseases) as well as the physiological processes such as learning and memory.[7,10,13–23] Carbon-11 has a short physical half-life of 20 minutes and efforts have been made towards the development of a fluorine-18 based PET radiotracer with a longer (110 min) physical half-life. Most of the investigated candidates thus far were structurally related to the ABP688 scaffold. Among the explored derivatives, the Pike group followed by the Ametamey group utilized the thiazole functionality and reported on highly potent analogues [^{18}F]-SP203 (Fig. 1),[24–26] and [^{18}F]-FTECMO (Fig. 1),[27] respectively, both of which exhibited defluorination *in vivo* in rats. Despite observed defluorination in rats and non-human primates, [^{18}F]-SP203 was explored in human subjects and showed limited radiodefluorination.[24] [^{18}F]-SP203 has less resemblance to the ABP688 manifold and exhibited superior binding affinity (IC_{50}) of 36 ± 9 pM. On the other hand, the structure of [^{18}F]-FTECMO differed from the structure of ABP688 in that the pyridine moiety from ABP688 was replaced by the thiazole functionality and showed a K_i value of 5.5 ± 1.1 nM. With the goal of further probing the thiazole functionality on the [^{11}C]-ABP688 scaffold and to ascertain whether a new ligand with improved *in vivo* binding properties could be generated, we sought to explore a new carbon-11 labelled ABP688 analogue, [^{11}C]-ThioABP. In effect, combining the ABP688 cyclohexenyl subunit labelled with carbon-11 with the more active thiazole component allowed for a new structural construct which could be a potentially useful mGluR5 imaging agent. We herein report the synthesis of ThioABP, the radiolabelling and pharmacological evaluation of [^{11}C]-ThioABP *in vitro* and *in vivo* as well as the

[a]*Centre for Radiopharmaceutical Sciences of ETH, PSI and USZ, Department of Chemistry and Applied Biosciences, ETH Zurich, Wolfgang-Pauli strasse 10, 8093 Zurich, Switzerland. E-mail: simon.ametamey@pharma.ethz.ch; Fax: +41 44 6331367; Tel: +41 44 6337463*

[b]*Centre for Radiopharmaceutical Sciences of ETH, PSI and USZ, Department of Nuclear Medicine, University Hospital Zurich, Rämistrasse 100, 8091 Zurich, Switzerland. E-mail: linjing.mu@usz.ch; Fax: +41 44 6331367; Tel: +41 44 2559687*

† Electronic supplementary information (ESI) available: NMR data for **5**, IC_{50} binding curves, HPLC traces are provided. See DOI: 10.1039/c2md20332d

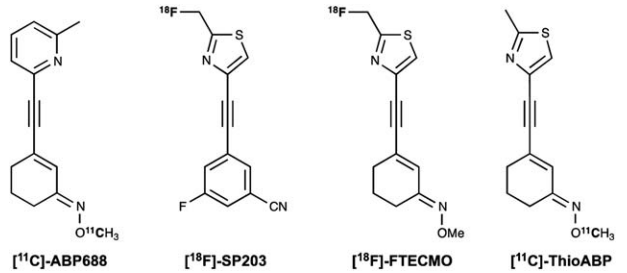

Fig. 1 Structures of [^{11}C]-ABP688 and thioazole containing PET radiotracers for imaging mGluR5.

comparative analysis of the *in vivo* PET scans of the two radiotracers [^{11}C]-ThioABP and [^{11}C]-ABP688.

Results and discussion

Syntheses of ThioABP and [^{11}C]-ThioABP

ThioABP was synthesized analogously to the synthesis of ABP688 and the synthetic scheme is depicted in Scheme 1.

Bromomethyl thiazole **2** was obtained by lithiation of the commercially available dibromothiazole **1** with *n*-butyllithium and concomitantly reacted with dimethyl sulfate in 38% yield (Scheme 1).[28] Sonogashira reaction of thiazole **2** with cyclohexenyl oxime **3** afforded hydroxy oxime **4** in 41%, which was used as a precursor for the radiolabelling. The corresponding standard reference, methyl oxime ether **5** (ThioABP) was synthesized from oxime **4** and methyliodide in a 32% yield. All compounds were characterized by proton and carbon NMR spectroscopy, IR and MS. The assignment of the oxime ether double bond configuration in **3** has been previously established.[29]

Radiolabelling of precursor **4** was performed in an automated Veenstra module. [^{11}C]-CO_2 was produced in the cyclotron *via* the ^{14}N(p,α)^{11}C nuclear reaction using a nitrogen gas target in the presence of 0.5% of oxygen. [^{11}C]-CO_2 was then reduced with hydrogen over RANEY® nickel to [^{11}C]-CH_4 followed by the reaction with I_2 at high temperature to yield [^{11}C]-CH_3I. Reaction with I_2 is repeated in the circulation mode and is the rate determining step for the carbon-11 labelling. Finally, [^{11}C]-ThioABP was radiosynthesized by bubbling of [^{11}C]-CH_3I through the reaction mixture of precursor **4** and NaH

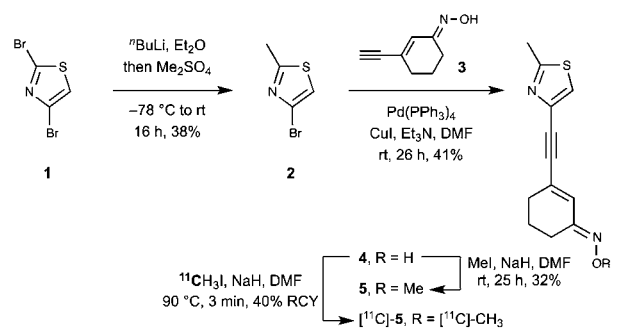

Scheme 1 Synthesis and radiolabelling of precursor **4** and the preparation of cold reference **5**.

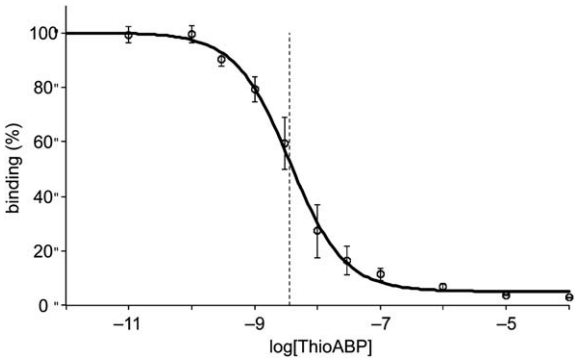

Fig. 2 [^{3}H]-ABP688 displacement curve for ThioABP. Three independent experiments were performed. The averaged values and their standard deviations are represented by symbols. Data were analysed by non-linear regression assuming one binding site (solid line curve). Fitted IC_{50} was 3.82 ± 1.55 nM (indicated by the dotted line).

in DMF at 90 °C (Scheme 1). Semi-preparative HPLC was used for the purification and [^{11}C]-ThioABP was formulated in 5% ethanol for subsequent *in vitro* and *in vivo* characterization. Co-injection with reference compound **5** confirmed the identity of the radiolabelled product [^{11}C]-**5** ([^{11}C]-ThioABP). In a typical experiment, the decay corrected radiochemical yield was around 40% and the specific activity of [^{11}C]-ThioABP was in the range of 80–250 GBq μmol^{-1} at the end of synthesis with >99% radiochemical purity. Notably, [^{11}C]-ThioABP was obtained as a mixture with a by-product, which was identified as a *Z*-isomer. The *E* : *Z* ratio of the formulated product [^{11}C]-ThioABP was >20 : 1 similar to that of [^{11}C]-ABP688.[2,30]

In vitro and *in vivo* evaluation of [^{11}C]-ThioABP

The lipophilicities of [^{11}C]-ABP688 and [^{11}C]-ThioABP were expected to be similar based on their calculated (clogP) values (2.4 and 2.3, respectively). The distribution coefficient log $D_{7.4}$ of [^{11}C]-ThioABP in octanol–phosphate buffer was 2.4 ± 0.1 ($n = 4$), identical to the log $D_{7.4}$ value reported for [^{11}C]-ABP688 (2.4 ± 0.1).[2]

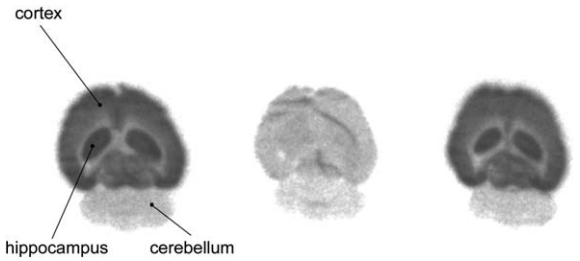

Fig. 3 *In vitro* autoradiography on rat brain slices under baseline and blocking conditions. Left: high radioactivity accumulation is observed in the brain regions with highest mGluR5 expression under baseline conditions (1 nM [^{11}C]-ThioABP); middle: complete blocking is achieved by co-incubation with cold ABP688 (100 nM); right: [^{11}C]-ThioABP shows selectivity for mGluR5 over mGluR1 as confirmed by co-incubation with excess mGluR1 antagonist JNJ16259685. *Note: Slices used for the experiment do not contain striatal brain regions. The slides correspond to the plates designated as PW116, bregma –3.10 mm in Paxinos and Watson, The Rat Brain Atlas, 1998 edition.*

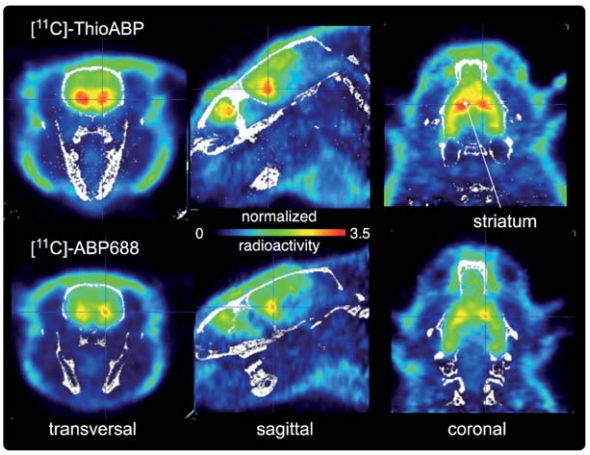

Fig. 4 [11C]-ThioABP and [11C]-ABP688 PET images of a rat (head). Images are averaged from 2 to 45 min after i.v. injection of 40.5 and 31.2 MBq of [11C]-ThioABP and [11C]-ABP688, respectively. Both tracers show the highest uptake in striatum, a region rich in mGluR5.

The binding affinity (K_i) of ThioABP towards mGluR5 was determined *via* a displacement assay with rat brain membranes using [3H]-ABP688. The K_i value was estimated from the IC_{50} value using the Cheng–Prusoff equation (see the Experimental section). Three independent experiments performed in triplicate revealed a favourable K_i of 1.9 ± 0.9 nM which is within the range required for an optimal mGluR5 PET tracer for imaging in the brain and comparable to that of ABP688 (2.4 nM).[2] The displacement curve showing the averaged values of three IC_{50} measurements is depicted in Fig. 2.

The high binding affinity of ThioABP measured in the displacement assay prompted us to further evaluate whether binding of [11C]-ThioABP was selective and specific for mGluR5. For this purpose, an *in vitro* autoradiography was performed on rat brain slices with [11C]-ThioABP under baseline (tracer only) and blocking (ABP688 or JNJ16259685) conditions (Fig. 3). Incubation of slices with 1 nM solution of [11C]-ThioABP resulted in a heterogeneous distribution of radioactivity with the highest accumulation in the regions where mGluR5 is highly expressed (*e.g.*, hippocampus and cortex) and background levels in cerebellum where mGluR5 expression is low.[21,31] Co-incubation of the brain slices with excess of ABP688 (100 nM) and 1 nM [11C]-ThioABP led to a significant reduction of radioactivity accumulation and a homogenous distribution, indicating saturation of available binding sites by excess ABP688 and therefore specificity of [11C]-ThioABP for mGluR5.

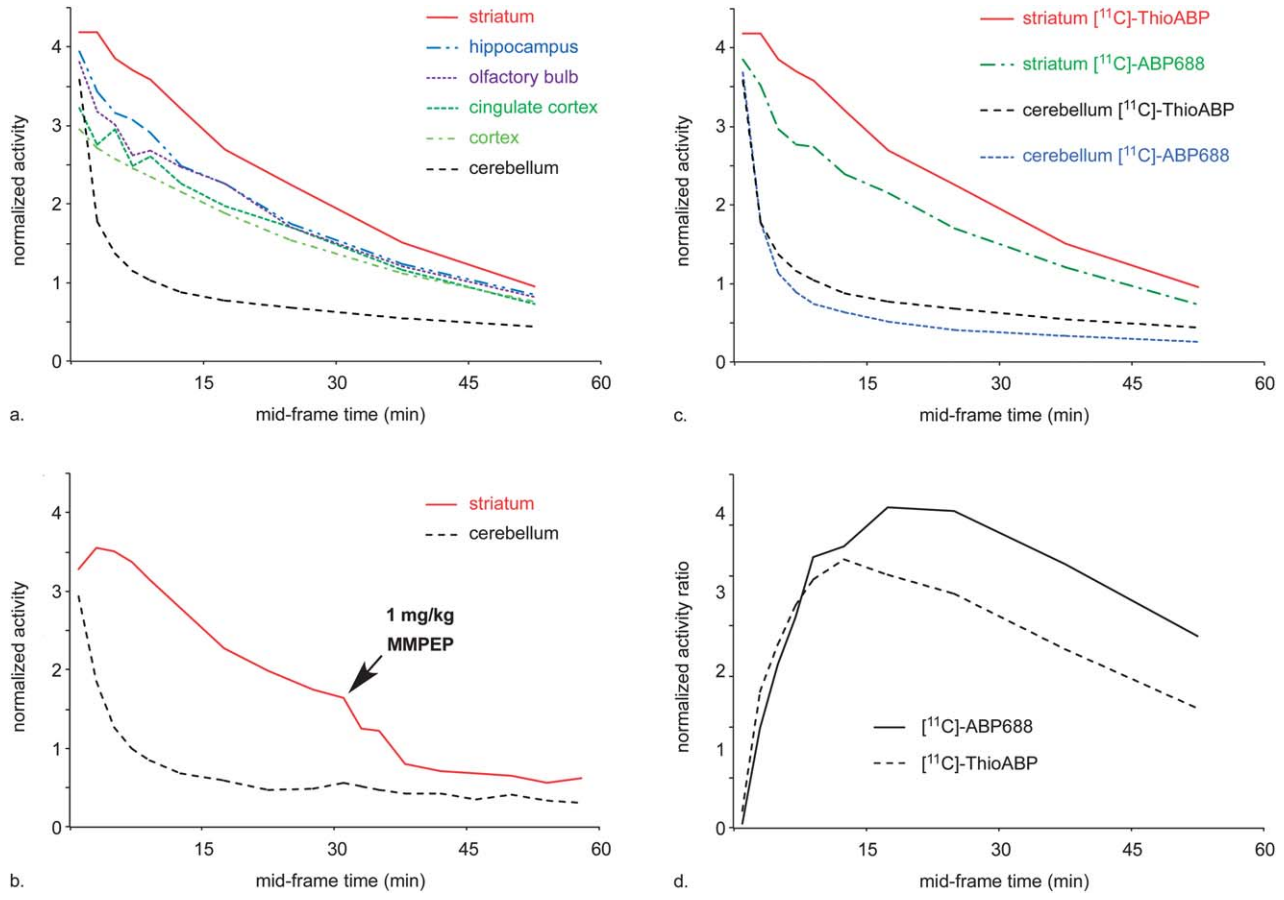

Fig. 5 Time–activity curves (TACs) for [11C]-ThioABP and [11C]-ABP688. (a): TACs for the *in vivo* dynamic PET scan with [11C]-ThioABP in rat, baseline heterogeneous activity distribution; (b): TACs for the *in vivo* dynamic PET displacement scan with [11C]-ThioABP, 1 mg kg^{-1} MMPEP 30 min p.i., reduction in activity uptake as a result of displacement with mGluR5 antagonist; (c): direct comparison of TACs for [11C]-ThioABP and [11C]-ABP688 in the brain regions of highest (striatum) and lowest (cerebellum) expression of mGluR5; (d): [11C]-ThioABP and [11C]-ABP688 ratios between specifically bound and free or non-specifically accumulated tracers in striatum and cerebellum.

On the other hand, application of 1 nM [^{11}C]-ThioABP together with an excess of mGluR1 antagonist, JNJ16259685 (100 nM), showed the same radioactivity distribution as under baseline conditions.

We next evaluated properties of [^{11}C]-ThioABP *in vivo*. Fig. 4 shows PET/CT images of rat head regions after [^{11}C]-ThioABP and [^{11}C]-ABP688 injections, respectively. [^{11}C]-ThioABP shows the same heterogeneous distribution pattern as [^{11}C]-ABP688 with highest uptake in brain regions with high mGluR5 expression (striatum, hippocampus and cortex) and low radioactivity in the cerebellum. This distribution pattern is in agreement with the results of an autoradiographic study *in vitro*.

The normalized time–activity curves (TACs) of [^{11}C]-ThioABP, obtained from the PET images, in mGluR5-rich brain regions and the cerebellum are shown in Fig. 5a. A displacement experiment was also conducted to investigate the specificity and reversibility of [^{11}C]-ThioABP binding to mGluR5. To this end, 1 mg kg^{-1} of mGluR5 antagonist MMPEP was injected i.v. 30 min after tracer application. As seen in Fig. 5b the application of MMPEP resulted in a reduction of radioactivity in mGluR5-rich regions to the level of radioactivity typically observed in the cerebellum, thus suggesting selective and reversible binding of [^{11}C]-ThioABP to mGluR5. The TACs of [^{11}C]-ThioABP and [^{11}C]-ABP688 were then compared to show a similar overall shape. Normalized radioactivity values for [^{11}C]-ThioABP were higher than those for [^{11}C]-ABP688 in the brain regions examined. For clarity, only the striatum and cerebellum are depicted in Fig. 5c. Fig. 5d depicts the respective ratios ((activity in striatum – activity in cerebellum)/activity in cerebellum) for the two radiotracers. At distribution equilibrium, this ratio becomes a constant for a radioligand that binds reversibly to its target and is taken as an estimate of the binding potential (BP), *i.e.*, the ratio between a specifically bound tracer and unbound or non-specifically accumulated tracer.[32,33] BP is dependent on the receptor density (B_{max}), receptor binding affinity (K_d) and non-specific tissue accumulation. Comparing the two scans, the ratio of the specific to free/non-specifically accumulated tracer was higher for [^{11}C]-ABP688 than for [^{11}C]-ThioABP (considering the data between 10 and 60 min p.i.). BP could not be estimated, because the equilibration between the specifically bound and free/non-specifically bound tracer was not reached within the scan duration of 60 min for either tracer.

Blood–brain barrier permeating radioactive metabolites generated by liver metabolism could contribute to background radioactivity in the brain. Blood samples drawn 10 min after tracer injection showed 37% of parent [^{11}C]-ThioABP and 63% of other more polar radio-metabolites. More importantly, 90% of intact parent radiotracer was detected in the brain sample at 10 min p.i. These results are comparable to the results obtained for [^{11}C]-ABP688, where 95% of brain radioactivity originated from the parent radiotracer 30 min after the [^{11}C]-ABP688 application.[2] In the rat brain homogenates, [^{18}F]-SP203 demonstrated significant radiodefluorination *in vivo*.[25] Therefore, [^{11}C]-ThioABP, analogous to [^{11}C]-ABP688 showed superior metabolic stability in comparison to [^{18}F]-SP203.

Conclusions

The structure of ThioABP was a combination of the thiazole component from highly potent fluorine-18 labelled mGluR5 PET tracers which underwent defluorination *in vivo* and cyclohexenyl carbon-11 labelled oxime bearing subunit from a clinically applied carbon-11 based mGluR5 PET tracer [^{11}C]-ABP688. Evaluation of [^{11}C]-ThioABP *in vivo* in a dynamic PET scan showed the highest activity uptake in striatum where mGluR5 is highly expressed. The specificity and reversibility of [^{11}C]-ThioABP binding to mGluR5 was also confirmed by the displacement study with the mGluR5 antagonist, MMPEP. In comparison to [^{11}C]-ABP688, an mGluR5 PET radiotracer applied clinically with success, [^{11}C]-ThioABP exhibited similar *in vitro* and *in vivo* profiles; however, [^{11}C]-ThioABP exhibited a slightly reduced ratio between the specifically bound and free/non-specifically accumulated tracer. The metabolic stability of [^{11}C]-ThioABP was comparable to that of [^{11}C]-ABP688. Overall, the similarity observed in the *in vivo* behaviour of the two tracers suggested that the introduction of the thiazole functionality did not improve the *in vivo* properties of the new thiazole based ligand.

Experimental

General techniques

All reactions requiring anhydrous conditions were conducted in flame-dried glass apparatus under an atmosphere of inert gas. All chemicals and anhydrous solvents were purchased from Aldrich or ABCR and used as received unless otherwise noted. Compounds **2**,[28] **3**,[29] and **4** (ref. 27) were prepared as previously described. The reported density values are for ambient temperature. [^{3}H]-ABP688 (2.405 GBq μmol^{-1}, 37 MBq mL^{-1} solution in EtOH) was obtained from AstraZeneca. Preparative chromatographic separations were performed on Aldrich Science silica gel 60 (35–75 μm) and reactions followed by TLC analysis using Sigma-Aldrich silica gel 60 plates (2–25 μm) with a fluorescent indicator (254 nm) and visualized with UV or potassium permanganate. Infrared spectra were recorded on a JASCO FT/IR 6200 (OmniLab) spectrometer using a chloroform solution of the compound. ^{1}H and ^{13}C NMR spectra were recorded in Fourier transform mode at the field strength specified on Bruker Avance FT-NMR spectrometers. Spectra were obtained from the specified deuterated solvents in 5 mm diameter tubes. Chemical shift in ppm is quoted relative to residual solvent signals calibrated as follows: $CDCl_3$ δ_H ($CHCl_3$) = 7.26 ppm, δ_C = 77.2 ppm. Multiplicities in the ^{1}H NMR spectra are described as: s = singlet, d = doublet, t = triplet, q = quartet, quint. = quintet, m = multiplet, b = broad; coupling constants are reported in Hz. Numbers in parentheses following carbon atom chemical shifts refer to the number of attached hydrogen atoms as revealed by the DEPT spectral editing technique. Electrospray (ES) mass spectra (LRMS) were obtained with a Micromass Quattro micro API LC and electrospray ionization and electrospray (ES) mass spectra (HRMS) were obtained with a Bruker FTMS 4.7 T BioAPEXII spectrometer. Ion mass/charge (m/z) ratios are reported as values in atomic mass units. Semi-preparative purification of radiolabelled material

was performed on a Merck-Hitachi L2130 system equipped with Elite LaChrom HITACHI L-2400 variable wavelength detector and a VEENSTRA VRM-202 radiation detector using a reverse phase column (C8 Waters Symmetry, 5 μm, 7.8 × 50 mm) and eluting with 0.1% aq. H_3PO_4 (solvent A) and acetonitrile (solvent B) as solvents and a gradient from 0 to 5 min 70% B; 5–10 min 30–50% B; 10–20 min 50% B at a flow rate of 4 mL min^{-1}. Analytical HPLC samples were analyzed by Agilent HPLC 1100 system equipped with a UV multi-wavelength detector and Raytest Gabi star radiation detector using a reverse phase column (ACE 111–0546, C18, 3 μm, 50 × 4.6 mm) and eluting with 45% aq. MeCN at a flow rate of 1 mL min^{-1}. Further information on a Veenstra automated module for the carbon-11 radio-labelling can be found online at: http://www.de.veenstranet.com.

Animals

Male Wistar rats were obtained from Charles River (Sulzfeld, Germany). Animal care and all experimental procedures were approved by the Cantonal Veterinary Office in Zurich, Switzerland. The animals were allowed free access to food and water.

Chemistry

(*E*)-3-((2-Methylthiazol-4-yl)ethynyl)cyclohex-2-enone *O*-methyl oxime (5). A flame dried round bottom flask was at ambient temperature under an atmosphere of N_2 charged with (*E*)-3-((2-methylthiazol-4-yl)ethynyl)cyclohex-2-enone oxime (70 mg, 0.30 mmol) and anhydrous *N*,*N*′-dimethylformamide (3 mL) was added and the clear yellow solution was then treated with sodium hydride 60% suspension in oil (14 mg, 0.36 mmol) in one portion and the resulting dark yellow mixture was stirred for 40 min. After this time the mixture was further treated with a solution of methyliodide (20 μL, 47 mg, 0.33 mmol, $d = 2.28$) in anhydrous *N*,*N*′-dimethylformamide (2 mL) dropwise over 4 min and the brown mixture was stirred for 24 h. After this time the mixture was quenched with saturated aq. $NaHCO_3$ (5 mL) and it was diluted with H_2O (5 mL) and EtOAc (10 mL) and the two layers were well shaken and separated. The aqueous phase was extracted with EtOAc (2 × 10 mL). The combined organic extracts were washed with H_2O (3 × 8 mL), brine (1 × 9 mL), dried (Na_2SO_4) and concentrated *in vacuo* to give the crude material as a brown oily residue (727 mg). The crude mixture was purified by chromatography on a silica gel column (eluting with 20% EtOAc–pentane) to afford the title compound (18.2 mg, 0.07 mmol, 32%) as a pale yellow solid: IR ($CDCl_3$) 2934, 1497, 1437, 1294, 1170, 1047, 919, 885, 868, 747 cm^{-1}; ^1H NMR (400 MHz, $CDCl_3$) δ 7.31 (s, 1H), 6.51 (s, 1H), 3.91 (s, 3H), 2.72 (s, 3H), 2.53 (m, 2H), 2.37 (m, 2H), 1.79 (quint, $J = 6.1$ Hz, 2H) ppm; ^{13}C NMR (100 MHz, $CDCl_3$) δ 165.9 (0), 155.6 (0), 136.9 (0), 130.3 (1), 127.5 (0), 122.7 (1), 89.8 (0), 87.0 (0), 62.1 (3), 29.6 (2), 22.3 (2), 21.0 (2), 19.4 (3) ppm; MS (ES+) *m*/*z* 247 $(M + H)^+$; HRMS (ESI) *m*/*z* 247.0899 (calcd for $C_{13}H_{15}N_2OS$: 247.0900).

Radiolabelling

(*E*)-3-((2-Methylthiazol-4-yl)ethynyl)cyclohex-2-enone *O*-^{11}C-methyl oxime ([^{11}C]-5). [^{11}C]-Methyliodide was produced *via* the nuclear reaction $^{14}N(p,\alpha)^{11}C$ as follows: the [^{11}C]-CO_2 formed was reduced to [^{11}C]-CH_4 by reduction using a RANEY® nickel catalyst and [^{11}C]-CH_4 was reacted with I_2 at 720 °C to yield [^{11}C]-CH_3I. [^{11}C]-Methyliodide was then bubbled through the heated (temperature of the reaction 90 °C) yellow mixture of (*E*)-3-((2-methylthiazol-4-yl)ethynyl)cyclohex-2-enone oxime (1.08 mg, 4.65 μmol) in anhydrous *N*,*N*′-dimethylformamide (0.2 mL) and sodium hydride (0.4 mL, $c = 1.7$ mg mL^{-1}) in anhydrous *N*,*N*′-dimethylformamide and the mixture was stirred for 3 min after which time it was diluted with 30% MeCN in 0.1% aq. H_3PO_4 (1.4 mL) and purified by HPLC semi-preparative chromatography. The collected product was diluted with H_2O (12 mL) and then passed through pre-conditioned (with EtOH 1 × 5 mL; then H_2O 1 × 5 mL) C18 light cartridge and the title compound was eluted with EtOH (0.5 mL) and the product was formulated by diluting with 9.5 mL of PEG : H_2O (1 : 1) solution. Specific activity was determined to be 80–250 GBq μmol^{-1} at the end of the synthesis and purity >99% in *E* : *Z* ratio higher than 20 : 1. However, the *E* : *Z* ratio of [^{11}C]-ThioABP varied and in some instances pure *E*-isomer was obtained. Variation was due to the peak overlap of *E*- and *Z*-isomers in semi-preparative HPLC. The total synthesis time from the end of bombardment was 35 min.

(*E*)-3-((6-Methylpyridin-2-yl)ethynyl)cyclohex-2-enone *O*-[^{11}C]-methyl oxime ([^{11}C]-ABP688). Radiolabelling was performed using the same module system as for the synthesis of [^{11}C]-**5** and as previously described.[2,30] Specific activity was determined to be >100 GBq μmol^{-1} at the end of the synthesis and purity >99% in an *E* : *Z* ratio higher than 10 : 1.

Pharmacological evaluation

Binding affinity. Brain membranes were prepared from Sprague Dawley rat brains as described previously.[29,34] Frozen membranes were thawed on ice and pelleted at 45 000× *g* at 4 °C for 5 min. The membranes were washed twice with HEPES buffer (30 mM HEPES, 110 mM NaCl, 5 mM KCl, 2.5 mM $CaCl_2$, 1.2 mM $MgCl_2$, pH 8 at 4 °C) and resuspended in HEPES buffer at a protein concentration of 1.3 mg mL^{-1}. The binding assay was performed as previously described.[29] In brief, brain membranes (0.1 mg protein) were incubated in triplicates at ambient temperature with 2 nM [^{3}H]ABP688 and ThioABP at concentrations between 10 pM and 100 μM in a total volume of 0.2 mL HEPES. ThioABP was diluted from a 1 mM ethanolic (50%) solution. The corresponding EtOH concentrations did not affect [^{3}H]ABP688 binding (data not shown). Nonspecific binding of [^{3}H]ABP688 was estimated with 100 μM MMPEP. After 45 min, the samples were filtered and the filters containing the membranes with bound [^{3}H]ABP688 were measured in a β-counter (Beckman LS6500). Bound [^{3}H]ABP688 (B, pmol per mg protein) was fitted with Excel solver to eqn (1) to estimate IC_{50}.

$$B = B_{min} + ((B_{max} - B_{min})/(1 + (C/IC_{50}))) \quad (1)$$

where *C* is the total ThioABP concentration, B_{max} is fitted maximal *B*, *i.e.*, the plateau in the *B*/log *C* plot at low log *C* and B_{min} is fitted minimal *B*, *i.e.*, the plateau at high log *C*. The inhibition constant K_i of ThioABP was estimated from IC_{50} and

K_d of ABP688 (1.7 ± 0.2 nM) (ref. 2) with the Cheng–Prusoff equation.

Determination of log *D*. The determination of log *D* value was performed using the shake-flask method as previously reported.[29,35] A formulated solution of [^{11}C]-ThioABP (*ca.* 4 MBq) was partitioned between phosphate buffer (pH 7.4) saturated with 1-octanol (500 μL) and 1-octanol saturated with phosphate (pH 7.4) buffer (750 μL). The washed octanol phase was divided into four individual aliquots (150 μL) and each was diluted with phosphate (pH 7.4) buffer saturated with 1-octanol (150 μL) and the two phases were shaken and radioactivity in each phase was measured in a γ-counter.

***In vitro* autoradiography.** Frozen horizontal brain slices (20 μm) from a male Wistar rat (535 g) adsorbed to SuperFrost Plus slides were thawed at ambient temperature and pre-incubated on ice for 10 min in HEPES buffer (see above) containing 0.1% bovine serum albumin (BSA). Excess solution was carefully removed and slides were incubated with 1 nM [^{11}C]-ThioABP alone or together with 100 μM ABP688 or 100 μM JNJ16259685 in HEPES buffer for 45 min at ambient temperature. After incubation, the solutions were decanted and the slides washed in ice cold HEPES buffer containing 0.1% BSA, and twice in HEPES buffer (3 minutes each) and finally dipped in H_2O. Dried slides were exposed to a phosphor imager plate for 30 min and the plate was scanned in a BAS5000 reader (Fuji).

***In vivo* PET/CT scans.** Rats were immobilized by anaesthesia with 2–3% isoflurane in oxygen/air on a GE Vista explore PET/CT scanner with the head in the field of view (axial field of view 4.8 cm). Body temperature was controlled with a rectal probe connected to a 37 °C air blower and respiratory frequency was monitored with a 1025T Small Animal Monitoring and Gating System from SA Instruments (Sony Brook, NY, USA). At the start of data acquisition 40.5 MBq (baseline scan) and 31.3 MBq (displacement experiment) of [^{11}C]-ThioABP, respectively, were injected into a tail vein, followed by 100 μL saline and data were collected in list mode for 60 min. For the displacement study, 1 mg kg^{-1} MMPEP in PEG : H_2O (1 : 1) was injected into the tail vein over 1 min starting 30 min after tracer injection. After the PET scans, a CT was performed for anatomical orientation. PET data were reconstructed with 2D ordered subset expectation maximization (2D OSEM) and analyzed with PMOD 3.2 (PMOD, Zurich, Switzerland). From the PET data, the measured radioactivity values expressed as Bq cm^{-3} were normalized to injected activity per gram body weight (Bq g^{-1}) and plotted against time.

Metabolite studies. Rats were injected as described above with 500 MBq of [^{11}C]-ThioABP. At 10 min p.i. the rat was sacrificed by decapitation and blood and urine were collected. The brain was carefully removed and homogenized in 2 mL phosphate buffered saline (pH 7.4). Plasma was separated from whole blood by centrifugation and brain homogenate plasma and urine were incubated with equal volumes of ice cold MeOH. Precipitated proteins were removed by centrifugation (4800 g, 5 min, 4 °C) and the step was repeated for the brain homogenate. Supernatants were analysed by radio-TLC (eluting with EtOAc : pentane 2 : 1).

Acknowledgements

Mr Bruno Mancosu is acknowledged for technical support with the carbon-11 module. Ms Claudia Keller is acknowledged for technical support in the PET lab. Dr Mark A. Sephton (ZHAW) is acknowledged for proofreading the manuscript. Prof. P. A. Schubiger is acknowledged for useful discussions.

Notes and references

1 S. M. Ametamey, M. Honer and P. A. Schubiger, *Chem. Rev.*, 2008, **108**, 1501–1516.
2 S. M. Ametamey, L. J. Kessler, M. Honer, M. T. Wyss, A. Buck, S. Hintermann, Y. P. Auberson, F. Gasparini and P. A. Schubiger, *J. Nucl. Med.*, 2006, **47**, 698–705.
3 S. M. Ametamey, V. Treyer, J. Streffer, M. T. Wyss, M. Schmidt, M. Blagoev, S. Hintermann, Y. Auberson, F. Gasparini, U. C. Fischer and A. Buck, *J. Nucl. Med.*, 2007, **48**, 247–252.
4 S. Hintermann, I. Vranesic, H. Allgeier, A. Bruelisauer, D. Hoyer, M. Lemaire, T. Moenius, S. Urwyler, S. Whitebread, F. Gasparini and Y. P. Auberson, *Bioorg. Med. Chem.*, 2007, **15**, 903–914.
5 V. Bruno, I. Ksiazek, G. Battaglia, S. Lukic, T. Leonhardt, D. Sauer, F. Gasparini, R. Kuhn, F. Nicoletti and P. J. Flor, *Neuropharmacology*, 2000, **39**, 2223–2230.
6 C. Burger, A. Deschwanden, S. Ametamey, A. Johayem, B. Mancosu, M. Wyss, G. Hasler and A. Buck, *Nucl. Med. Biol.*, 2010, **37**, 845–851.
7 N. Calcinaghi, R. Jolivet, M. T. Wyss, S. M. Ametamey, F. Gasparini, A. Buck and B. Weber, *J. Cereb. Blood Flow Metab.*, 2011, **31**, e1–e10.
8 C. DeLorenzo, J. S. D. Kumar, J. J. Mann and R. V. Parsey, *J. Cereb. Blood Flow Metab.*, 2011, **31**, 2169–2180.
9 A. Deschwanden, B. Karolewicz, A. M. Feyissa, V. Treyer, S. M. Ametamey, A. Johayem, C. Burger, Y. P. Auberson, J. Sovago, C. Stockmeier, A. Buck and G. Hasler, *Am. J. Psychiatry*, 2011, **168**, 727–734.
10 B. Ouattara, L. Gregoire, M. Morissette, F. Gasparini, I. Vranesic, G. Bilbe, D. R. Johns, A. Rajput, O. Hornykiewicz, A. H. Rajput, B. Gomez-Mancilla and T. D. Paolo, *Neurobiol. Aging*, 2011, **32**, 1286–1295.
11 V. Treyer, J. Streffer, M. T. Wyss, A. Bettio, S. M. Ametamey, U. Fischer, M. Schmidt, F. Gasparini, C. Hock and A. Buck, *J. Nucl. Med.*, 2007, **48**, 1207–1215.
12 M. T. Wyss, S. M. Ametamey, T. Valerie, B. Andrea, M. Blagoev, L. J. Kessler, C. Burger, B. Weber, M. Schmidt, F. Gasparini and B. Alfred, *NeuroImage*, 2007, **35**, 1086–1092.
13 P. J. Conn and J. P. Pin, *Annu. Rev. Pharmacol. Toxicol.*, 1997, **37**, 205–237.
14 L. P. Daggett, A. I. Sacaan, M. Akong, S. P. Rao, S. D. Hess, C. Liaw, A. Urrutia, C. Jachec, S. B. Ellis, J. Dreessen, T. Knopfel, G. B. Landwehrmeyer, C. M. Testa, A. B. Young, M. Varney, E. C. Johnson and G. Velicelebi, *Neuropharmacology*, 1995, **34**, 871–886.
15 F. Dorri, D. R. Hampson, A. Baskys and J. M. Wojtowicz, *Exp. Neurol.*, 1997, **147**, 48–54.

16 Y. M. Lu, Z. Jia, C. Janus, J. T. Henderson, R. Gerlai, J. M. Wojtowicz and J. C. Roder, *J. Neurosci.*, 1997, **17**, 5196–5205.
17 K. Ossowska, J. Konieczny, J. Wardas, M. Pietraszek, K. Kuter, S. Wolfarth and A. Pilc, *Amino Acids*, 2007, **32**, 179–188.
18 J. P. Pin and R. Duvoisin, *Neuropharmacology*, 1995, **34**, 1–26.
19 A. Ritzen, J. M. Mathiesen and C. Thomsen, *Basic Clin. Pharmacol. Toxicol.*, 2005, **97**, 202–213.
20 R. Shigemoto, A. Kinoshita, E. Wada, S. Nomura, H. Ohishi, M. Takada, P. J. Flor, A. Neki, T. Abe, S. Nakanishi and N. Mizuno, *J. Neurosci.*, 1997, **17**, 7503–7522.
21 R. Shigemoto and N. Mizuno, *Handb. Chem. Neuroanat.*, 2000, **18**, 63–98.
22 Y. Tanabe, M. Masu, T. Ishii, R. Shigemoto and S. Nakanishi, *Neuron*, 1992, **8**, 169–179.
23 P. K. Todd, K. J. Mack and J. S. Malter, *Proc. Natl. Acad. Sci. U. S. A.*, 2003, **100**, 14374–14378.
24 A. K. Brown, Y. Kimura, S. S. Zoghbi, F. G. Simeon, J. S. Liow, W. C. Kreisl, A. Taku, M. Fujita, V. W. Pike and R. B. Innis, *J. Nucl. Med.*, 2008, **49**, 2042–2048.
25 H. U. Shetty, S. S. Zoghbi, F. G. Simeon, J. S. Liow, A. K. Brown, P. Kannan, R. B. Innis and V. W. Pike, *J. Pharmacol. Exp. Ther.*, 2008, **327**, 727–735.
26 F. G. Simeon, A. K. Brown, S. S. Zoghbi, V. M. Patterson, R. B. Innis and V. W. Pike, *J. Med. Chem.*, 2007, **50**, 3256–3266.
27 C. A. Baumann, L. Mu, N. Wertli, S. D. Krämer, M. Honer, P. A. Schubiger and S. M. Ametamey, *Bioorg. Med. Chem.*, 2010, **18**, 6044–6054.
28 U. Karama and G. Höfle, *Eur. J. Org. Chem.*, 2003, 1042–1049.
29 C. A. Baumann, L. Mu, S. Johannsen, M. Honer, P. A. Schubiger and S. M. Ametamey, *J. Med. Chem.*, 2010, **53**, 4009–4017.
30 F. Gasparini, Y. Auberson, L. Kessler and S. M. Ametamey, WO2005/030723, PCT/EP2004/010743, 2005.
31 R. Shigemoto, S. Nomura, H. Ohishi, H. Sugihara, S. Nakanishi and N. Mizuno, *Neurosci. Lett.*, 1993, **163**, 53–57.
32 M. Fumita and R. B. Innis, In Vivo *Molecular Imaging: Ligand Development and Research Applications*, American College of Neuropsychopharmacology, 2002.
33 R. B. Innis, V. J. Cunningham, J. Delforge, M. Fujita, A. Gjedde, R. N. Gunn, J. Holden, S. Houle, S. C. Huang, M. Ichise, H. Iida, H. Ito, Y. Kimura, R. A. Koeppe, G. M. Knudsen, J. Knuuti, A. A. Lammertsma, M. Laruelle, J. Logan, R. P. Maguire, M. A. Mintun, E. D. Morris, R. Parsey, J. C. Price, M. Slifstein, V. Sossi, T. Suhara, J. R. Votaw, D. F. Wong and R. E. Carson, *J. Cereb. Blood Flow Metab.*, 2007, **27**, 1533–1539.
34 S. M. Sephton, P. Dennler, D. Leutwiler, L. Mu, C. A. Wanger-Baumann, R. Schibli, S. D. Krämer and S. M. Ametamey, *Am. J. Nucl. Med. Mol. Imaging*, 2012, **2**, 14.
35 A. A. Wilson, L. Jin, A. Garcia, J. N. DaSilva and S. Houle, *Appl. Radiat. Isot.*, 2001, **54**, 203–208.

